Water mass transformation in the North Atlantic over 1985?2002 simulated in an eddy-permitting model

R. Marsh, S. A. Josey, A. J. G. Nurser, B. A. de Cuevas, A. C. Coward

Ocean Science Discussions, 2, 63–104, 2005
www.ocean-science.net/osd/2/63/
SRef-ID: 1812-0822/osd/2005-2-63
European Geosciences Union

Ocean Science Discussions

Water mass transformation in the North Atlantic over 1985–2002 simulated in an eddy-permitting model

R. Marsh, S. A. Josey, A. J. G. Nurser, B. A. de Cuevas, and A. C. Coward

Southampton Oceanography Centre, Southampton, United Kingdom

Received: 11 February 2005 – Accepted: 23 March 2005 – Published: 11 April 2005

Correspondence to: R. Marsh (rma@soc.soton.ac.uk)

Abstract

Water mass transformation in the North Atlantic is examined in an eddy-permitting simulation with the OCCAM ocean general circulation model, forced by realistic surface fluxes over the period 1985–2002. Three regions are considered: the Subtropics, the Mid-latitudes and the Northeast Atlantic. The oceanic boundaries of each region coincide with hydrographic sections occupied in recent years. These regions broadly represent the formation sites of Subtropical Mode Water (STMW) and Subpolar Mode Water (SPMW). A water mass budget is obtained for each region and year. Terms in the budget comprise surface-forced transformation rates, boundary exchanges and unsteadiness. Unsteadiness is relatively small, so that regional net water mass transformation is largely balanced by net boundary exchanges. Transformation rates due to mixing are then obtained as the difference between net and surface transformation rates.

Transports at the boundaries are compared with recent observations, and reasonable agreement is obtained. For the period 1985–1993, model surface transformation rates are broadly in agreement with equivalent rates computed using the globally-balanced SOC fluxes of heat and freshwater, derived from ship observations. In each Atlantic region, surface transformation rates reach 10–15 Sv, based on both model and SOC fluxes. Higher spatial and temporal resolution in the OCCAM surface fluxes may improve the realism of surface transformation rates in some regions, notably the Labrador Sea. However, the unrealistic location of the North Atlantic Current too far south leads to spurious surface heating east of the Grand Banks in OCCAM. Period-mean transformation rates due to mixing reveal the formation of intermediate waters in each region due to the "consumption" of lighter and denser waters formed by surface fluxes, and are comparable with recent inverse estimates. There is, however, strong interannual-to-decadal variability in the consumption rates. In the subtropics, STMW consumption rates co-vary with STMW formation rates. In the subpolar gyre, anomalies in SPMW consumption rate appear to lag anomalies in the surface formation rate

OSD

2, 63–104, 2005

by up to 4 years.

1. Introduction

Progressive surface density gain along upper circulation pathways in the North Atlantic leads to the formation of two principal water masses: Subtropical Mode Water (STMW) in the western subtropical gyre and Subpolar Mode Water (SPMW) in the eastern subpolar gyre. Increases in surface density are principally due to winter cooling (McCartney and Talley, 1984). Across the subtropical and mid-latitude North Atlantic at the end of winter, deep mixed layer waters are subducted into the permanent thermocline (Marshall et al., 1993) and are subsequently modified through interior mixing (Tziperman, 1986). At higher latitudes, in the Labrador and Nordic Seas, Labrador Sea Water (LSW) and Greenland Sea Deep Water are the end-product of deep convective mixing and lateral mixing between boundary currents and the gyre interior. A full description of water mass transformation requires accurate knowledge of both the surface fluxes and interior mixing processes. Observationally, transformation rates can be estimated from tracers (Rhein et al., 2002), or by inversions of measured transports across hydrographic sections (Ganachaud, 2003; Lumpkin and Speer, 2003). In addition, Ocean General Circulation Models (OGCMs) have proved to be useful tools in the exact determination of water mass transformation (Nurser et al., 1999), although the problem of water mass unsteadiness in models is a recognised drawback (Nurser and Marsh, 1998).

Interannual-to-decadal variability in water mass transformation is suggested by evidence for changes in the volume and properties of STMW (Alfutis and Cornillon, 2001; Kwon and Riser, 2004), SPMW (Thierry et al., 2004) and LSW (Dickson et al., 1996). Such variability is most directly a consequence of changes in local surface fluxes, which have been associated with leading modes of atmospheric variability such as the North Atlantic Oscillation (NAO). Secular trends in water mass transformation may also be associated with climate change (Dickson et al., 2003). The role of diapycnal mixing in

OSD
2, 63–104, 2005

water mass variability is much less clear. Regionally-integrated diapycnal fluxes due to mixing have been evaluated in OGCMs under climatological forcing and boundary conditions (e.g. Nurser et al., 1999) and most recently in coupled climate models (e.g. Haines and Old, 2005). Mixing may be especially strong in the vicinity of fronts and eddies. In the low resolution OGCMs previously used to diagnose water mass transformation rates (e.g. Nurser et al., 1999), fronts are too broad and eddies are parameterized. Experiments with an eddy-resolving ocean model configured in an idealized basin showed that eddies enhance subduction rates by a factor of ∼2 (Hazeleger and Drijfhout, 2000), and studies of water mass formation are now being carried out with eddy-resolving OGCMs configured in realistic geometry (e.g. Valdivieso da Costa et al., 2005). The mixing-driven "destruction" or "consumption" of SPMW also supplies nutrients to surface waters, helping to maintain high primary production in the subpolar gyre (Oschlies, 2002).

Combining advances in both resolution and forcing, we diagnose water mass transformation in an eddy-permitting OGCM forced by realistic surface fluxes over 1985–2002. We validate the transport and transformation of water masses in the model by comparison with selected observations, and by considering simulated variability alongside observational evidence for recent changes in the North Atlantic. The paper is arranged as follows. The model and simulation are described in Sect. 2. Diagnostic procedures are outlined in Sect. 3. Results are presented in Sect. 4. In Sect. 5 the results are discussed in comparison with other model studies and observations.

2. The model

The data used in this analysis is output from the latest run of the Ocean Circulation and Climate Advanced Model (OCCAM) 1/4° global ocean model (Saunders et al., 1999). This version combines 1/4°×1/4° horizontal (eddy-permitting) resolution with high vertical resolution – 66 levels with 14 in the top 100 m. Improved physics packages have been introduced as well as a sophisticated sea ice model with elastic-viscous-

OSD
2, 63–104, 2005

plastic (EVP) dynamics (Hunke and Dukowicz, 1997) and three layer thermodynamics. The initial tracer fields (potential temperature and salinity) were interpolated from the WOCE Special Analysis Centre climatology (Gouretski and Jancke, 1998) for most of the World's oceans together with tracer distributions for the Arctic. See http://www/soc.soton.ac.uk/JRD/OCCAM/ for full details.

Several features of the new model allow us to capture the spatial and temporal variability of the upper ocean. Key to this is a comprehensive set of high frequency atmospheric fields together with a realistic bulk formulation of atmospheric forcing. Input fields of wind speed, air temperature, specific humidity, sea level pressure, cloudiness, precipitation and short wave radiation are used, together with the model top level temperature, to compute the heat and freshwater forcing to be applied at each time step. The input data were provided through the NCEP/NCAR reanalysis project (Kalnay et al., 1996). The method used to calculate the fluxes from these data is described in Large et al. (1997, Appendix A). Improvements in model physics and the use of realistic, balanced surface forcing have led to improved simulation of the Atlantic thermohaline circulation compared to an earlier OCCAM simulation in which sea surface temperatures and salinities were restored to monthly climatological values (Hirschi et al., 2003).

The model was first integrated from its initial state for four model-years using atmospheric fields from 1985 to 1988. The final state from this run was then used to initialise an 18-year integration using atmospheric fields from 1985 to 2002. Running totals of the model variables and forcing fields were accumulated during the model run and output at the end of each month. These have been used to calculate the monthly mean fields for this analysis.

3. Diagnostics

We use the well-established water mass transformation diagnostic first introduced by Walin (1982) and originally applied to the North Atlantic by Speer and Tziperman

(1992). We diagnose the transformation of water mass partioned according to potential density (σ_0). In the North Atlantic, water masses can be unambiguously defined according to σ_0, although this approach is problematic elsewhere in the World Ocean, notably in the Southern Ocean. Using the index k to denote progressively higher σ_0, we can relate a rate of change in the regional volume, $V(\sigma_{k-1}, \sigma_k)$, of a layer bounded by density surfaces σ_{k-1}, σ_k and σ_{k-1}, σ_k, and open boundaries, to surface fluxes, diapycnal mixing and net advection across the boundaries:

$$\partial_t V(\sigma_k, \sigma_{k-1}) = (\psi_{net}(\sigma_k) - \psi_{net}(\sigma_{k-1})) - (G(\sigma_k) - G(\sigma_{k-1})), \quad (1)$$

where $\psi_{net}(\sigma_k)$ is a net density-partitioned overturning streamfunction, integrated down from the surface (taking all open boundaries into account), and $G(\sigma_k)$ is the net diapycnal volume transport (positive towards higher density) within the region, across the surface defined by $G(\sigma_k)$. Averaging over one or more annual cycles, the left hand side of Eq. (1) gives a measure of regional water mass unsteadiness. The transport $G(\sigma_k)$ is a net "water mass transformation rate", due to a combination of surface fluxes and mixing:

$$G(\sigma_k) = G_{surf}(\sigma_k) + G_{mix}(\sigma_k), \quad (2)$$

where $G_{surf}(\sigma_k)$ and $G_{mix}(\sigma_k)$ are the transformation rates due to surface fluxes and mixing respectively. In OCCAM, we compute $G_{surf}(\sigma_k)$ from monthly datasets, on the model (i,j) grid, as:

$$G_{surf}(\sigma_k) = \frac{1}{(\sigma_k - \sigma_{k-1})} \sum_{m=1}^{12} \Delta t \sum_{i,j} \left[\Delta A_{i,j} f_{i,j,m} \Pi\left(\sigma_k, \overline{\sigma_{i,j,surf}}\right)\right] \quad (3)$$

obtained by summing (over partitions of gridbox area, $\Delta A_{i,j}$, and monthly periods, Δt) $f_{i,j,m}$, the monthly-mean surface flux of density due to net surface heat and salt fluxes, where $\Pi\left(\sigma_k, \overline{\sigma_{i,j,surf}}\right)$ is a sampling function which takes the value 1 if $\sigma_{k-1} \leq \overline{\sigma_{i,j,surf}} \leq \sigma_k$, otherwise the value 0, given $\overline{\sigma_{i,j,surf}}$, the monthly-mean surface density.

OSD
2, 63–104, 2005

We diagnose fluxes for a selection of sections through the model grid which coincide as closely as possible with hydrographic lines occupied during WOCE and planned under the auspices of CLIVAR. The sections (see Fig. 1) are as follows:

1. A5, along 26° N
2. A3, along 36° N except in the east where the section terminates at the Spanish coast
3. A25, at 41.5° N from the Spanish coast to 20° W, thereafter towards Cape Farewell, Greenland
4. AR7W, from southwest Greenland to the Labrador Shelf
5. The Extended Ellett Line, from the Scottish Hebrides via Rockall to South Iceland along 20° W, continued from West Iceland to Greenland along 64° N ("EEL-64N")

Sections 2–5 coincide as close as possible with actual occupations. For convenience, the model "A5" section follows 26° N, rather than following exactly the actual section, which deviates between 24° N and 26.5° N. To close mass budgets, we also include short sections across the Straits of Gibraltar (GibSt) and, for the purposes of examining Labrador Sea Water formation, the Canadian Archipelago (CA). The sections are indicated on Fig. 1. We thus identify three regions enclosed by sections as follows:

1. A5-A3-GibSt: "Subtropics" Box
2. A3-AR7W-A25: "Mid-latitudes" Box
3. A25-EEL-64N: "NE Atlantic" Box

For these regions, we compare surface forced water mass transformation in OCCAM with corresponding values obtained from the Southampton Oceanography Centre (SOC) flux dataset for the common period 1985–1993. Note we have used both the original version of the SOC flux dataset (Josey et al., 1999, referred to as unadjusted

SOC here), in which there is a global mean ocean heating bias of 30 Wm^{-2}, and a subsequent adjusted version in which this bias has been removed using inverse analysis with hydrographic constraints (Grist and Josey, 2003). We also obtain integral mixing as a residual in the water mass budget, and compare the mean and variability in water mass transformation through mixing with that due to surface fluxes.

4. Results

The results are presented in four stages, progressing as follows. First we present and discuss property-binned transports across the sections, and evaluate the model using relevant observations. We then use the model results to obtain net water mass transformation rates, accounting for unsteadiness. Next, we compute surface transformation rates in OCCAM, and compare these with estimates computed with the two versions of the SOC flux dataset (Josey et al., 1999; Grist and Josey, 2003). Finally we examine the difference between net and surface transformation rates, and attribute this to the total effect of mixing.

4.1. Period-mean transports across sections

Figure 2 shows 1985–2002 mean transports across each section, partitioned according to potential temperature (θ) and salinity (S). For direct comparison with two of the sections, Fig. 3 shows the transports estimated from recent occupations of A5 (Lavín et al., 2003) and A25 (Álvarez et al., 2002). Transports and properties on the other sections are discussed in the context of published observations, where available. Tables 1 and 2 list the corresponding total light and dense flows, and the net barotropic transport, for each section.

Model transport across A5 (Fig. 2a) features strong northward flux in the temperature range 23–26°C and the salinity range 35.8–36.4 psu, corresponding to the Florida Current. Across a broader range of θ, northward and southward transports are typically

separated in salinity by 0.2–0.4 psu, due to the effects of net evaporation and recirculation north of A5. The export of North Atlantic Deep Water (NADW) comprises of strong southward fluxes at 34.8–35.2 psu and 2–6°C. Antarctic Bottom Water (AABW) provides the northward flux of ∼3 Sv at 34.8–35.0 psu and 1–2°C. Much of the observed northward and southward-recirculating transport at A5 (Fig. 3a) is at higher salinity, by ∼0.2 psu. It is not clear why the equivalent model transports are fresher than the observations, although there are several possible causes. As the 1992 occupation of A5 took place in June, the discrepancy may be partly due to seasonal bias. Near-surface transports (of lighter waters) may be sensitive to differences between the climatological annual-mean winds used to compute Ekman transport (for the observations) and the reanalysed (6-hourly) winds applied in the model. The evaporation and precipitation rates used in OCCAM may also introduce regional salinity biases. In addition to the salinity offset, observed southward fluxes of NADW are located at lower temperature, by around 1°C. As a consequence, the AABW transport evident in Fig. 2a is not clear in Fig. 3a. This is because the observed AABW more closely "overlaps" in (θ, S) space with the stronger southward transport of NADW, and is obscured. Despite these differences, the level of agreement between simulated and observed transports is encouraging.

Progressing to A3 (Fig. 2b), northward transports have shifted towards lower temperature and higher salinity due to strong heat loss and evaporation in the Sargasso Sea recirculation gyre. Although the 36° N section was not occupied during the study period, the strength and structure of transport is broadly consistent with an earlier 1981 occupation (Roemmich and Wunsch, 1985). Some of the northward transport across A3 at high salinity (above 36 psu) is due to the additional influence of Mediterranean Water (MW). Exchange at the Straits of Gibraltar (Fig. 2c) is somewhat stronger than observations would suggest. As period-means, the inflow of Atlantic Water is 1.17 Sv and the outflow of MW is 1.12 Sv. These compare with recent estimates of 0.78±0.47 Sv inflow and 0.67±0.26 Sv outflow (Tsimplis and Bryden, 2000). The stronger exchange in OCCAM may be related to missing tidal effects, although the estimates based on

current meter measurements are also contingent on cross-strait and vertical sampling strategies. The salinity of outflowing MW, in the range 38.0–38.4 psu, is close to observations (see Fig. 6 of Tsimplis and Bryden, 2000).

At A25 (Fig. 2d), the majority of northward transport is restricted to 6–15°C, and shifted by up to 0.8 psu towards lower salinity, relative to northward transports at A3. Compared to observations (Fig. 3b), the southward-flowing NADW in OCCAM is warmer by ∼2°C and more saline by ∼0.2 psu. These systematic differences in dense water mass properties are likely due to excessive entrainment of surrounding water into overflow waters, a problem that is not unusual in level-coordinate ocean models (Marsh et al., 1996). Property differences are actually somewhat smaller in the present OCCAM experiment, compared to simulations with coupled climate models such as HadCM3 (in which NADW is too saline by ∼0.5 psu, a longstanding model error, see Wood et al., 1999; Wu et al., 2004).

Transport across AR7W (Fig. 2e) is strikingly cold and fresh, incorporating southward transport of water close to the freezing point. Strong northward and southward fluxes occur in adjacent temperature classes. Strong variability in the formation and transport of LSW limit the long-term representativeness of individual AR7W occupations. However, AR7W has been occupied at least annually since 1990, and from what has been observed (e.g. Pickart et al., 2002), our period-mean transports appear realistic. The temperature and salinity ranges of southward flows, −2 to 4°C and 33.4 to 35.2 psu respectively, are in close agreement with observations at AR7W (e.g. Fig. 8 of Pickart et al., 2002).

At EEL-64N (Fig. 2f), substantial northward transport persists at relatively high temperature (6–12°C) while the majority of southward transport is in the temperature range 3–6°C. The warm northward fluxes are located on the EEL half of the amalgamated section. A large fraction of the cold southward flux is made up of waters derived from overflows through the Denmark Straits (DS) and the Faroe Bank Channel (FBC). Girton et al. (2001) recently estimated the DS overflow, just south of the sill, to be steady at 3.8±0.8 Sv, while Hansen et al. (2001) observe the FBC overflow gradually decreasing

OSD
2, 63–104, 2005

from ∼1.9 Sv in the early 1990's. Added to an extra ∼1 Sv across the ridge between Iceland and the Faroes, the combined ∼6.7 Sv of overflow in recent years is comparable with an earlier estimate of 5.6 Sv by Dickson and Brown (1994). South of DS at around 64° N, and across the 20°W part of EEL south of Iceland, Dickson and Brown (1994) estimate that the overflows (denser than σ_0=27.8 kg m^{-3}) have strengthened by entrainment to 5.1 Sv and 3.5 Sv respectively, giving a total of 8.6 Sv. In OCCAM, total southward transport across EEL-64N is 14.9 Sv, of which 9.3 Sv lies in temperature classes below 5°C and at potential density above around 27.6 kg m^{-3} (transport at slightly higher temperature/lower density is associated with the East Greenland Current). We therefore conclude that the model overflows across EEL-64N are realistic in strength, although too light by around 0.2 kg m^{-3}.

Figure 4 shows transports partitioned according to potential density, σ_0, in "bins" of width 0.1 kg m^{-3}. Fluxes through the Gibraltar Straits are included with fluxes across A3. The sections A25 and AR7W are likewise considered together, as well as A25 separately. The two curves shown in each plot indicate a range of values due to interannual variability over 1985–2002, according to positive and negative excursions from the mean by two standard deviations. The close proximity of upper and lower bounds on transport confirm the relative steadiness of transports, averaged over 18 years. The upper panels show fluxes, the lower panels show cumulative transport, obtained by summing the fluxes, from low to high values of σ_0. The density of northward flows progressively increases across Figs. 4a–4e, while the density of southward flows is relatively unchanged. In fact, the southward flows increase in density between A25-AR7W and A3-GibSt, by just ∼0.1 kg m^{-3}. This is largely due to gradual southward penetration of insufficiently dense overflows, although entrainment of denser AABW and MW into the NADW layer will also tend to increase the density of that layer (see the reduction in AABW flux, comparing Figs. 4b and 4c). The profiles of cumulative transport provide four views of the thermohaline circulation, declining in strength towards the high latitude sinking regions. The non-zero residual values of cumulative transport at high density (see also Table 1) correspond to a long-term barotropic component of the

circulation due to Bering Strait throughflow (period-mean value is ∼0.8 Sv) and the net exchange of freshwater across the ocean surface (in particular, ∼0.2 Sv is gained in the Arctic).

4.2. Net water mass transformation in the three enclosed regions

Figure 5 shows period-mean volume fluxes as a function of σ_0, in the three bounded regions. In Fig. 5a, we show differences in cumulative transports at the bounding sections shown in Fig. 4, due to the net import or export of water masses. Positive values indicate a volume flux from low to high values of σ_0. The maximum in this flux increases northwards, from 24.7 kg m^{-3} in the Subtropical Box, to 25.8 kg m^{-3} in the Mid-latitudes Box, to 27.3 kg m^{-3} in the NE Atlantic Box.

In Fig. 5b, we show the period-mean trend per region, expressed as a volume flux. This trend is most conspicuous at high density, due to the problem of model unsteadiness. The volume fluxes associated with this trend are negative at most densities, for all three regions. This indicates that the ocean in each region is getting slightly lighter over 1985–2002. The envelope of two standard deviations is relatively wide, due to strong inter-annual variability in water masses, especially in the thermocline range of $25<\sigma_0<27.8$, for which the period-mean trend is closer to zero. This suggests that the trend is only partly a model artefact, and may also result from inter-annual variability in the surface fluxes.

In Fig. 5c, we show the net water mass transformation rate, computed by subtracting the volume flux associated with trend from that due to the net input. As the trend is only substantial at high density, the net transformation rate is close to the volume flux in Fig. 5a. This net water mass transformation rate is due to the combined effects of surface fluxes and mixing, the former of which we now evaluate.

OSD
2, 63–104, 2005

4.3. Water mass transformation due to surface fluxes

We now compare water mass transformation rates obtained from OCCAM with values diagnosed using two versions of an independent dataset, the SOC flux climatology (Josey et al., 1999; Grist and Josey, 2003). Note that we have used SOC rather than NCEP as our comparison dataset because fluxes derived from the NCEP meteorological variables have been used to force the model, thus the NCEP fluxes are not independent. Some differences between the values obtained using OCCAM and NCEP fluxes would occur, but only due to differences between sea surface temperatures and sea ice cover in OCCAM, compared with corresponding fields prescribed for the NCEP reanalysis model.

Figure 6 shows surface flux-induced water mass transformation rates (G_{surf}) in OCCAM and computed using the SOC heat and freshwater fluxes, for each of the three Atlantic regions. We also now include surface water mass transformation rates in the Labrador Sea, as far north as the Canadian Archipelago, for reasons that will become evident. Figure 6a shows the OCCAM average over 1985–2002. The red, green and blue curves in Fig. 6a broadly resemble those in Fig. 5c, as water mass transformation is strongly linked to air-sea exchanges of heat and freshwater.

We compare surface transformation rates in OCCAM with equivalent rates determined using the SOC fluxes, for the common period of 1985–1993. Figures 6b and 6c show the transformation rate for this period in OCCAM, and using the adjusted SOC fluxes (Grist and Josey, 2003). There is good general agreement in the three Atlantic boxes. Differences between the two sets of curves are summarised as follows:

1. in the Subtropical Box, there is stronger transformation at lower density (peak ~13 Sv at σ_0=25.6 kg m^{-3}) in OCCAM, compared with the SOC fluxes (peak ~12 Sv at σ_0=26.0 kg m^{-3});

2. in the Mid-latitudes Box, there is stronger transformation at higher density (peak ~12 Sv at σ_0=26.6 kg m^{-3}) in OCCAM, compared with the SOC fluxes (peak

~13 Sv at σ_0=26.2 kg m^{-3});

3. in the NE Atlantic Box, transformation rates in OCCAM are almost double those obtained with the SOC fluxes, although there is less surface transformation at σ_0>27.6 kg m^{-3} in OCCAM, compared with the SOC fluxes.

Despite the broad agreement found in the three main boxes, there is a significant difference between OCCAM and SOC surface transformation rates in the Labrador Sea. In OCCAM, transformation rates peak at 15 Sv at σ_0=27.4 kg m^{-3}, and remain high (14 Sv) at σ_0=27.6 kg m^{-3}, while with the SOC fluxes transformation rates reach only 0.3 Sv. This large discrepancy is clearly associated with differences in surface net heat flux (see below). The OCCAM peak transformation rates are in excess of an estimated ~6 Sv peak rate obtained from NCEP reanalysis data for a larger region (40–70° W, 50–65° N) and averaged over 1958–1999 (Khatiwala et al., 2005). The average surface transformation rate over 1985-93 was, however, probably higher than the long-term average. Rhein et al. (2002) use an inventory of chlorofluorocarbon to estimate a minimum formation rate of LSW over 1988-94 of 8.1–10.8 Sv. Based on these observed estimates, we consider that the OCCAM peak rate of 15 Sv is probably too large by about 50%. Compared with satellite data, winter sea surface temperatures in OCCAM are biased high by 2–4°C in the Labrador Sea (manscript in prep.), which would enhance surface heat loss during cold air outbreaks.

Noting that the SOC fluxes have been globally adjusted, we also consider the unadjusted fluxes. Figure 6d shows the transformation rate obtained with the unadjusted SOC fluxes (Josey et al., 1999). The level of agreement with OCCAM in the three main boxes is now significantly poorer than before which is not surprising given that the unadjusted SOC fluxes are known to significantly underestimate the ocean heat loss to the atmosphere (Josey et al., 1999). However, the transformation rates found using unadjusted SOC are in better agreement with OCCAM in a few limited cases, for example at low density in the Mid-latitudes Box. This is consistent with the findings of Grist and Josey (2003) who note that the unadjusted SOC fluxes are in better agreement than

the adjuted ones with measurements made using research buoys in the eastern subtropical gyre, which is the source for the negative value of transformation at low density in the Mid-latitude Box.

To further investigate the differences between Figs. 6b–6d, we examine the 1985–1993 average net surface heat flux. Figure 7 shows the annual mean net heat flux in OCCAM (Fig. 7a), and for adjusted and unadjusted SOC fluxes (Figs. 7b and 7c). A striking feature in the OCCAM fluxes, is a broad area of strong heat gain, up to 100 Wm^{-2}, east of the Grand Banks centered on about (40° W, 48° N). This feature is absent from the SOC fluxes, and other major datasets that we have investigated including both the NCEP/NCAR and ECMWF reanalyses (not shown). This is largely because the model North Atlantic Current is located about 5° too far south in longitude range 30–45° W. This problem is not unusual in level coordinate ocean models (Marsh et al., 1996). Under the surface forcing scheme employed in the model, the unrealistically cold waters in this region are strongly heated by warmer overlying air, primarily through sensible and latent heat exchange, resulting in the abnormal pattern of heat gain.

Significant differences between OCCAM and SOC are found in some other regions but these may be indicative of problems with the SOC fields. The OCCAM heat fluxes reach greater negative extrema over the Gulf Stream, the Irminger Sea, and in the Labrador Sea. In particular, we note strong surface cooling in the northwest Labrador Sea which is largely absent in the SOC fluxes. As this region contains very few ship observations it is likely that the SOC heat loss is too weak in the Labrador Sea. The difference between OCCAM and SOC surface fluxes in the Labrador Sea is the major source of disagreement in surface transformation rates. Furthermore, although global adjustment of the SOC fluxes ensures sufficient basin-scale heat loss to balance the observed heat transport, a comparison of Figs. 7a and 7b suggests that heat loss is probably too widespread in the adjusted climatology. Both OCCAM and the unadjusted fluxes (Fig. 7c) are characterised by weak net surface heating across the subtropical gyre, south of a line stretching roughly from Florida to the Iberian peninsula. Excess net

OSD
2, 63–104, 2005

cooling across the subtropical gyre in the adjusted climatology leads to strong surface water mass transformation rates at higher density in the Subtropics Box, compared to OCCAM (see Figs. 6b and 6c). These results are consistent with the conclusion reached by Grist and Josey (2003), following comparisons with research buoy measurements, that the adjustment procedure leads to too great a gain in heat loss in the eastern subtropical North Atlantic and insufficient gain on the western side of the basin.

More generally, discrepancies between surface transformation rates obtained with OCCAM and SOC fluxes may arise for a variety of reasons:

1. Runoff is neglected in the calculation with SOC fluxes, but is implicitly included in the OCCAM surface freshwater flux. This may explain why transformation rates in the Mid-latitudes Box (strongly influenced by Canadian runoff) are more negative at low density.

2. The monthly-mean OCCAM fluxes include the effects of synoptic time and space scales, whereas these effects are probably under-sampled in the SOC fluxes. This may explain generally highly and "sharper" maxima in the OCCAM transformation rates, associated with narrow boundary currents and eddies.

3. The globally-adjusted SOC fluxes may still contain regional biases as discussed by Grist and Josey (2003).

4. The atmospheric data and bulk formulae used in the surface forcing of OCCAM may also introduce biases to the OCCAM fluxes, relative to the SOC fluxes.

Detailed investigation of the above issues is beyond the scope of the present paper. Our main conclusion is that, with the exception noted above, transformation rates obtained with OCCAM and adjusted SOC fluxes are in broad agreement.

We now consider OCCAM water mass formation rates in the three Atlantic regions plus the Labrador Sea, over 1985–2002. Formation rates in the Labrador Sea are included here to provide additional evidence of model realism over the simulation period,

as discussed below. Figure 8 shows Hovmuller plots of annual surface flux-driven formation rate in each σ_0-interval over ranges corresponding to formation of the densest water masses in each region. In the Subtropics, surface formation takes place above about σ_0=25.6 kg m^{-3} (Fig. 8a). The 18° Water found in the western subtropical gyre occupies the density range 26.4<σ_0<26.6 kg m^{-3}. Formation rates in this range are relatively weak and intermittent, with less water being formed in the latter part of the period considered (1995–2002). In the Mid-latitudes (Fig. 8b), the surface destruction and formation of water mass has shifted by ∼0.5 kg m^{-3}, and substantial formation rates are now found in the range 26.6<σ_0<27.1 kg m^{-3}. In the NE Atlantic Box (Fig. 8c), water mass destruction and formation is more coherent than in the two other regions, being well defined in the ranges 26.6<σ_0<27.2 kg m^{-3} and 27.2<σ_0<27.6 kg m^{-3} respectively. A similarly coherent picture emerges for the Labrador Sea (Fig. 8d), with destruction over 26.7<σ_0<27.4 kg m^{-3} and formation over 27.4<σ_0<28.0 kg m^{-3}. Also evident in Fig. 8d is a decadal transient in surface formation at σ_0>27.7 kg m^{-3}, with formation rate in the "dense LSW" range 27.8<σ_0<27.9 kg m^{-3} notably exceeding 4 Sv in 1990.

We now consider the total formation of four principal water masses:

1. "STMW1" in the Subtropics: σ_0>26.4 kg m^{-3}
2. "STMW2" in the Mid-latitudes: σ_0>26.6 kg m^{-3}
3. SPMW in the NE Atlantic: σ_0>27.2 kg m^{-3}
4. LSW in the Labrador Sea: σ_0>27.7 kg m^{-3}.

Figure 9 shows time series of the annual formation rate for each of these water masses. The variability evident in Fig. 8 is now more clearly revealed on interannual and decadal timescales. LSW formation reaches a peak in the early 1990's. This transient episode is well established from repeated hydrographic surveys of the Labrador Sea (Dickson et al., 1996). Also revealed in Fig. 9 is strong variability in the formation of STMW2

in the Mid-latitudes Box and SPMW in the NE Atlantic Box. STMW1 formation in the Subtropics Box is relatively weak and declines over most of the period. This is consistent with direct evidence for a relatively low and declining volume of this water mass over the same period (Kwon and Riser, 2004). Aside from the effects of surface fluxes, water masses are modified by mixing, which is the process we consider next.

4.4. Water mass transformation due to mixing

We obtain transformation rates due to "total" mixing as the difference between net and surface forced transformation rates. Total mixing is dominated by explicit diapycnal mixing, although it also includes the effects of cabbeling, due to isopycnal mixing, and the additional diapycnal velocity due to non-linearities in the equation of state (McDougall 1991). Figure 10 shows the transformation rates due to mixing in the three regions. In the Subtropics Box (Fig. 10a), the mixing curve is alternately positive and negative, as one would expect of diapycnal mixing, acting to transform light and dense waters towards intermediate density. This occurs over three density ranges: $22.0<\sigma_0<26.4\,\mathrm{kg\,m^{-3}}$; $26.4<\sigma_0<27.7\,\mathrm{kg\,m^{-3}}$; $27.7<\sigma_0<28.6\,\mathrm{kg\,m^{-3}}$. In the Mid-latitudes Box (Fig. 10b), the residual mixing curve appears more positive than negative, implying overall density gain. This is possibly a consequence of cabbeling through isopycnal mixing, either across the strong near-surface fronts in the region, or between warm, saline Mediterranean Water and surrounding cooler, fresher waters at intermediate depths. We cannot, however, rule out limitations in our methodology. Possible reasons for this positive bias are outlined in the Discussion. Despite this positive offset, mixing in the Mid-latitudes Box acts to transform light and dense waters to intermediate density in the broad range $22.0<\sigma_0<27.1\,\mathrm{kg\,m^{-3}}$. In the NE Atlantic Box (Fig. 10c), we again see that mixing has a net positive effect, but we also find an overall transformation to intermediate density in the range $25.7<\sigma_0<27.4\,\mathrm{kg\,m^{-3}}$.

We now consider the annual water mass formation rates due to mixing. Figure 11 shows Hovmuller plots of these formation rates over 1985–2002, across a wide range of density. The formation and destruction of water in different density classes, due

to mixing, is now clear. In the Subtropics Box (Fig. 11a), there is a broad swathe of formation in the intermediate density range $24.2<\sigma_0<25.6\,\mathrm{kg\,m^{-3}}$. This formation is at the expense of lighter water and denser water. The denser water is strongly "consumed" in the range $25.6<\sigma_0<26.6\,\mathrm{kg\,m^{-3}}$, which includes light STMW. At higher density, mixing leads to weaker formation in the density class $26.7<\sigma_0<27.5\,\mathrm{kg\,m^{-3}}$. At high density the alternate "bands" of strong formation and destruction reveal vigorous mixing of NADW, AABW and MW in the density range $27.6<\sigma_0<28.8\,\mathrm{kg\,m^{-3}}$. Similar swathes of formation and consumption are clear in the Mid-latitudes Box (Fig. 11b) and the NE Atlantic Box (Fig. 11c), with strong consumption rates in density ranges corresponding to STMW and SPMW respectively.

We next consider time series of annual mixing-driven formation rates, over 1985–2002, for each region and water mass (as Fig. 9), with the exception of LSW. In the case of LSW, we consider mixing of the dense variety ($27.8<\sigma_0<27.9\,\mathrm{kg\,m^{-3}}$) in the Mid-latitudes Box, based on evidence in Fig. 11b. The mixing-driven formation rates shown in Fig. 12 (solid curves) are generally negative, indicating consumption of each water mass within the region of formation (in the case of STMW1, STMW2 and SPMW) and in the adjacent region (in the case of LSW). Furthermore, strong interannual-to-decadal variability in the consumption rates largely matches that seen in the surface-driven formation rates (dotted curves in Fig. 12), most clearly in the case of STMW1 and STMW2 (Fig. 12a). This suggests that much of the subtropical mode water formed through surface heat and freshwater exchange is consumed in the same year and region. If this consumption is largely due to entrainment of water into the mixed layer, then the strong variability is likely linked (as is variability in formation rates) to large inter-annual fluctuations in winter mixed layer depth.

Some of the variability in consumption rates of SPMW and LSW (Fig. 12b) may be related to variability in surface formation rates over preceding years. For example, the strongest consumption rate in the NE Atlantic Box, ~11 Sv in 1998, lags four years behind a peak in SPMW formation rate of ~17 Sv in 1994. This time lag could correspond to a timescale of recirculation within the eastern subpolar gyre. Finally, we

OSD
2, 63–104, 2005

note net consumption in the density range $27.8<\sigma_0<27.9\,\mathrm{kg\,m^{-3}}$, over 1990–1997 in the Mid-latitudes Box. This may be related to the arrival in this region of newly-formed anomalous LSW, with a lag of around 1 year suggested by peaks in formation and consumption rate in 1990 and 1991 respectively. Further to the evidence for formation of the anomalous LSW, southward transport across AR7W over 1989–1995 is dominated by export of ~15 Sv in the density range $\sigma_0>27.8\,\mathrm{kg\,m^{-3}}$ (see Marsh et al., 2005). The inference is that the anomalously dense LSW rapidly mixes with surrounding waters in the mid-latitude North Atlantic.

5. Summary and discussion

We have diagnosed North Atlantic water mass transformation in an eddy-permitting ocean simulation forced by observed fluxes for the period 1985–2002. The large-scale circulation is similar to that estimated from observations at two repeat WOCE sections, in the subtropics and at mid-latitudes. We selected four basin-wide sections which have been occupied in recent years and are central to ongoing efforts to monitor the thermohaline circulation. These sections bound three regions of the North Atlantic: the Subtropics, Mid-latitudes and the Northeast Atlantic. The regions broadly represent the formation sites of Subtropical Mode Water and Subpolar Mode Water. Partitioning diapycnal fluxes in potential density, a water mass budget is obtained for each region and year. Terms in the budget comprise surface-forced transformation rates, boundary exchanges and unsteadiness. Property-binned transports across the bounding sections compare favourably with available observations and the thermohaline circulation is realistically vigorous. We find a small degree of unsteadiness at high density, probably related to excessive mixing in the overflows between the Fram Strait and Cape Farewell. Overall, there is a good balance between the formation, transport and consumption of water masses throughout the simulation. The most notable Atlantic variability during 1985–2002, associated with the episode of strong renewal of Labrador Sea Water during 1989–1994 (Dickson et al., 1996), is well simulated.

For a common period 1985–1993, model surface transformation rates are compared with equivalent rates computed using the adjusted SOC climatology (Grist and Josey, 2003) – globally-balanced fluxes of heat and freshwater which are derived from ship observations. There is an overall reasonable agreement between the two sets of transformation rates. However, compared to surface transformation rates computed from the flux dataset, those in the model reach more extreme maxima in the subtropics, the northeast Atlantic and the Labrador Sea. This is consistent with more extreme heat loss in these regions of OCCAM. Most crucial in the context of water mass transformation at LSW densities, strong heat loss in the northwest Labador Sea of OCCAM is largely absent in the SOC fluxes. This feature of the OCCAM simulation is consistent with a similar pattern of surface net heat flux obtained with NCEP reanalysis data (Pickart et al., 2002). The weak heat loss in the Labrador Sea in the SOC climatology is unsurprising given that very few ship observations are available for this region (see Fig. 2 of Josey et al., 1999).

We further note that transformation rates obtained with the adjusted SOC fluxes are generally shifted towards higher density. This is particularly the case in the subtropics, and may be associated with "over-adjustment" of the SOC fluxes in this region. This is most evident in the eastern subtropical gyre, where net surface cooling in the adjusted SOC fluxes is inconsistent with research buoy measurements of net warming (Grist and Josey, 2003). However, we also note incorrect positioning of the North Atlantic Current in OCCAM, which is located too far south to the east of the Grand Banks. This leads to unrealistically strong surface heating in the model of cold surface waters advected into the region by the Labrador Current.

Few other model studies of the recent ocean circulation and water mass transformation have been undertaken. Gulev et al. (2003) report a longer simulation than ours, using an Atlantic sector implementation of the SPEM ocean model at resolution of $\sim 1.2^{\circ}$, spanning 1958–1997. While their simulation spans more decadal variability, notably the effects of a low-to-high transition of the NAO-index, the mean state is rather unrealistic due to weak overturning and heat transport. Using the same model, Beismann

and Barnier (2004) obtain an overturning circulation more realistic in mean strength and variability, through improved representation of dense overflows. Using an adjoint approach to ocean state estimation (the ECCO project), Stammer et al. (2002) have established a benchmark for assimilation of WOCE data into an OGCM. However, constraints on surface fluxes and low resolution (2° horizontal over ±80° in latitude with 22 levels in the vertical) restrict heat transport in the Atlantic sector of the original ECCO state estimation to only around half of hydrographic estimates (Stammer et al., 2003). More recently, closer agreement with estimates of global ocean heat transport have been obtained in a further ECCO state estimation using 1° resolution (Stammer et al., 2004). These progressive improvements in the ECCO results highlight the importance of realistic surface fluxes and up to eddy-permitting resolution - as used here - for better representation of the large-scale circulation and surface water mass transformation.

The most uncertain component in water mass transformation, both observationally and in models, is due to mixing. While the mixing transformation rate curves in OCCAM are broadly similar to those obtained in previous model studies (e.g. Nurser et al., 1999), we can now compare our results with recent inverse estimates of interior diapycnal volume transports by Lumpkin and Speer (2003), henceforth LS, who considered three boxes similar to the ones we have employed. Comparisons are clearest for surface and thermocline waters in the subtropics. In their "Subtropical" box, LS estimate diapycnal transports (positive towards decreasing neutral density) which vary from a minimum of −7.5±1.5 Sv in their "Surface" layer (σ_0<26.0 kg m^{-3}) to a maximum of 7.5±3.5 Sv in their "Thermocline" layer (26.0<σ_0<27.1 kg m^{-3}). Noting our opposite sign convention, these extremes compare well to OCCAM "Subtropics" box values of 7±1 Sv (at σ_0=24.2 kg m^{-3}) and −10±2 Sv (at σ_0=25.6 kg m^{-3}) – see Fig. 10a. The implied mixing-driven formation rates are ∼15 Sv in LS (24.7<σ_0<26.4 kg m^{-3}) and ∼17 Sv in OCCAM (24.2<σ_0<25.6 kg m^{-3}). The "Subpolar" box of LS is displaced further north than our "Mid-latitudes" box and includes the Labrador Sea, while their "Overflow" box includes broadly the northern half of our "NE Atlantic" box. In their Subpolar box, LS estimate three distinct maxima and minima in diapycnal transport, with

notably a maximum of 2±1 Sv at σ_0=27.1 kg m^{-3} and a minimum of around −2±1 Sv at the density of LSW. This is in broad agreement with mixing transformation rates in the Mid-latitudes box of OCCAM, which features a minimum of −6±3 Sv at σ_0=26.7 kg m^{-3} and a maximum of around 6.5±3 Sv at σ_0=27.7 kg m^{-3}. Given the divergence of diapycnal transports across these density ranges, both LS and OCCAM suggest that mixing consumes SPMW and LSW at mid-latitudes, at rates of ∼4 Sv in LS and ∼12.5 Sv in OCCAM, although this comparison is compromised by substantial differences between areal coverage of the LS Subpolar Box and the OCCAM Mid-latitudes Box. The Overflow box of LS is dominated by a maximum in the density range for bottom waters and a minimum in the density range of upper deep waters. Mixing transformation rates in the NE Atlantic Box of OCCAM are considerably different from those in the Overflow Box of LS. In particular, the diapycnal transport estimates of LS imply ∼7 Sv formation of "Lower Deep" waters through mixing of "Upper Deep" and "Bottom" waters in the Overflow Box. Mixing rates at high density in OCCAM may be inaccurate for reasons associated with our offline method of diagnosis:

1. neglect of the correlation between transport and fluxes, and density, at timescales less than a month
2. neglect of sea ice effects on surface heat and freshwater fluxes
3. approximation of annual trends, by taking the difference between January monthly-mean density-partitioned volumes

A solution to this problem is exact "online" computation of diapycnal fluxes and water mass transformation. This is a challenging prospect, and has only been attempted once before to our knowledge (Nurser et al., 1999).

In OCCAM, there is strong interannual-to-decadal variability in the consumption rates of STMW, SPMW and LSW. In the subtropics, anomalies in STMW formation rate are largely offset by similar anomalies in consumption rate, in the same year. Coincidence of strong formation and consumption rates in a given year is probably due to the link

between surface density flux and winter mixed layer deepening at the regional scale, and does not negate the possibility for an oceanic "memory" of anomalous surface fluxes in preceding years. Haines and Old (2005) find that surface-formed STMW anomalies are re-entrained into the mixed layer after typically 5 years. To the extent that STMW is formed and consumed in the same region, we cannot identify when water masses formed in a given year are consumed. In the subpolar gyre, however, the peak SPMW consumption rate appears to lag anomalously strong surface formation by 4 years. This may reflect clearer separation of formation and consumption sites, or a weaker physical link between processes of formation and consumption, for SPMW, compared to STMW. Furthermore, consumption of anomalous LSW in the western subpolar gyre takes place after formation in the Labrador Sea, with an identifiable lag between strongest formation and consumption rates of 1 year.

Acknowledgements. This work was supported by the "Large Scale Long Term Ocean Circulation" and "Ocean Variability and Climate" Core Strategic Programmes of the UK Natural Environment Research Council. The A5 and A25 datasets were kindly provided by H. Bryden and M. Álvarez.

References

Alfultis, M. A. and Cornillon, P.: Annual and interannual changes in the North Atlantic STMW layer properties, J. Phys. Oceanogr., 31, 2066–2086, 2001.

Álvarez, M., Bryden, H. L., Pérez, F. F., Ríos, A. F., and Rosón, G.: Physical and biogeochemical fluxes and net budgets in the Subpolar and Temperate North Atlantic, J. Mar. Res., 60, 191–226, 2002.

Beismann, J.-O. and Barnier, B.: Variability of the meridional overturning circulation of the North Atlantic: sensitivity to overflows of dense water masses, Ocean Dynamics, 54, 92–106, 2004.

Curry, R. G. and McCartney, M. S.: Ocean gyre circulation changes associated with the North Atlantic Oscillation, J. Phys. Oceanogr., 31, 3374–3400, 2001.

Dickson, R. R. and Brown, J.: The production of North Atlantic Deep Water: Sources, rates and pathways, J. Geophys. Res., 99, 12 319–12 341, 1994.

Dickson, R. R., Lazier, J., Meincke, J., Rhines, P., and Swift, J.: Long-term coordinated changes in the convective activity of the North Atlantic, Prog. Oceanogr., 38, 241–295, 1996.
Dickson, R. R., Curry, R., and Yashayaev, I.: Recent changes in the North Atlantic, Phil. Trans. R. Soc. Lond. A, 361, 1917–1934, 2003.
Ganachaud, A.: Large-scale mass transports, water mass formation, and diffusivities estimated from World Ocean Circulation Experiment (WOCE) hydrographic data, J. Geophys. Res., 108, C7, 3213, doi:10.1029/2002JC001565, 2003.
Gouretski, V. V. and Jancke, K.: A new World Ocean climatology: Optimal interpolation of historical and WOCE hydrographic data on neutral surfaces, WOCE Rep. 162/98 (Available from WOCE Special Analysis Centre, Max Planck Institute, Hamburg, Germany), 1998.
Grist, J. P. and Josey, S. A.: Inverse analysis adjustment of the SOC air-sea flux climatology using ocean heat transport constraints, J. Climate, 20, 3274–3295, 2003.
Gulev, S. K., Barnier, B., Knochel, H., and Molines, J.-M.: Water Mass Transformation in the North Atlantic and Its Impact on the Meridional Circulation: Insights from an Ocean Model Forced by NCEP–NCAR Reanalysis Surface Fluxes, J. Climate, 16, 3085–3110, 2003.
Haines, K. and Old, C.: Diagnosing Natural Variability of North Atlantic Water Masses in HadCM3, J. Climate, in press, 2005.
Hansen, B., Turrell, W. R., and Østerhus, S.: Decreasing overflow from the Nordic seas into the Atlantic Ocean through the Faroe Bank channel since 1950, Nature, 411, 927–930, 2001.
Hazeleger, W. and Drijfhout, S. S.: Eddy subduction in a model of the subtropical gyre, J. Phys. Oceanogr., 30, 677–695, 2000.
Hirschi, J., Baehr, J., Marotzke, J., Stark, J., Cunningham, S., and Beismann, J.-O.: A monitoring design for the Atlantic meridional overturning circulation, Geophys. Res. Lett., 30, 1413, doi:10.1029/2002GL016776, 2003.
Hunke, E. C. and Dukowicz, J. K.: An elastic-viscous-plastic model for sea ice dynamics, J. Phys. Oceanogr., 27, 1849–1867, 1997.
Josey, S. A., Kent, E. C., and Taylor, P. K.: New insights into the ocean heat budget closure problem from analysis of the SOC air-sea flux climatology, J. Climate, 12, 2856–2880, 1999.
Kalnay, E., Kanamitsu, E., Kistler, M. et al.: The NCEP/NCAR reanalysis project, Bull. Amer. Meteor. Soc., 77, 437–495, 1996.
Khatiwala, S., Schlosser, P., and Visbeck, M.: Rates and mechanisms of water mass transformations in the Labrador Sea as inferred from tracer observations, J. Phys. Oceanogr., in press, 2005.

Kwon, Y.-O. and Riser, S. C.: North Atlantic Subtropical Mode Water: A history of ocean-atmosphere interaction 1961–2000, Geophys. Res. Lett., 31, L19307, doi:10.1029/2004GL021116, 2004.
Large, W. G., Danabasoglu, G., and Doney, S. C.: Sensitivity to Surface Forcing and Boundary Layer Mixing in a Global Ocean Model: Annual-Mean Climatology, J. Phys. Oceanogr., 27, 2418–2446, 1997.
Large, W. G. and Nurser, A. J. G.: Ocean surface water mass transformation, in: Ocean Circulation and Climate: Observing and Modelling the Global Ocean, edited by: Siedler, G., Church, J. and Gould, J., San Diego CA, Academic Press., 317–336 (International Geophysics Series No. 77), 2001.
Lavín, A. M., Bryden, H. L., and Parrilla, G.: Mechanisms of heat, freshwater, oxygen and nutrient transports and budgets at 24.5° N in the subtropical North Atlantic, Deep-Sea Res., 50, 1099–1128, 2003.
Lumpkin, R. and Speer, K.: Large-scale vertical and horizontal circulation in the North Atlantic Ocean, J. Phys. Oceanogr., 33, 1902–1920, 2003.
Marsh, R., Roberts, M. J., New, A. L., and Wood, R. A.: An intercomparison of a Bryan-Cox-type ocean model and an isopycnic ocean model. Part II: The subtropical gyre and meridional heat transport, J. Phys. Oceanogr., 26, 1528–1551, 1996.
Marsh, R., de Cuevas, B. A., Coward, A. C., Bryden, H. L., and Álvarez, M.: Thermohaline circulation at three key sections in the North Atlantic over 1985–2002, Geophys. Res. Lett., in press, 2005.
Marshall, J. C., Nurser, A. J. G., and Williams, R. G.: Inferring the subduction rate and period over the North Atlantic, J. Phys. Oceanogr., 23, 1315–1329, 1993.
McCartney, M. S. and Talley, L. D.: Warm-to-cold conversion in the northern North Atlantic Ocean, J. Phys. Oceanogr., 14, 922–935, 1984.
McClaren, A. J. and Williams, R. G.: Interannual variability in the thermodynamics of subduction over the North Atlantic, J. Phys. Oceanogr., 31, 3284–3294, 2001.
McDougall, T. J.: Parameterizing mixing in inverse models, Dynamics of Oceanic Internal Gravity Waves, edited by: Müller, P. and Henderson, D. Proc. Sixth. 'Aha Huliko'a Hawaiian Winter Workshop, University of Hawaii at Manoa, 355–386, 1991.
Nurser, A. J. G. and Marsh, R.: Water mass transformation theory and the meridional overturning streamfunction, International WOCE Newsletter, No. 31, 36–39, 1998.
Nurser, A. J. G., Marsh, R., and Williams, R. G.: Diagnosing water mass formation from air-sea

fluxes and surface mixing, J. Phys. Oceanogr., 29, 1468–1487, 1999.
Oschlies, A.: Nutrient supply to the surface waters of the North Atlantic: A model study, J. Geophys. Res., 107, doi:0.1029/2000JC000275, 2002.
Pickart, R. S., Torres, D. J., and Clarke, R. A.: Hydrography of the Labrador Sea during Active Convection, J. Phys. Oceanogr., 32, 428–457, 2002.
Rhein, M., Fischer, J., Smethie, W. M., Smythe-Wright, D., Weiss, R. F., Mertens, C., Min, D.-H., Fleischmann, U., and Putzka, A.: Labrador Sea Water: pathways, CFC-inventory and formation rates, J. Phys. Oceanogr., 32, 648–665, 2002.
Roemmich, D. and Wunsch, C.: Two transatlantic sections: meridional circulation and heat flux in the subtropical North Atlantic Ocean, Deep-Sea Res., 32, 619–664, 1985.
Saunders, P. M., Coward, A. C., and de Cuevas, B. A.: The Circulation of the Pacific Ocean seen in a Global Ocean Model (OCCAM), J. Geophys. Res., 104, C8, 18 281–18 299, 1999.
Speer, K. and Tziperman, E.: Rates of water mass formation in the North Atlantic Ocean, J. Phys. Oceanogr., 22, 93–104, 1992.
Speer, K.: A note on average cross-isopycnal mixing in the North Atlantic Ocean, Deep Sea Res., 44, 1981–1990, 1997.
Stammer, D., Wunsch, C., Giering, R., Eckert, C., Heimbach, P., Marotzke, J., Adcroft, A., Hill, C. N., and Marshall, J.: The global ocean circulation during 1992–1997, estimated from ocean observations and a general circulation model, J. Geophys. Res., 107, C9, 3118, doi:10.1029/2001JC000888, 2002.
Stammer, D., Wunsch, C., Giering, R., Eckert, C., Heimbach, P., Marotzke, J., Adcroft, A., Hill, C. N., and Marshall, J.: Volume, heat, and freshwater transports of the global ocean circulation 1993–2000, estimated from a general circulation model constrained by World Ocean Circulation Experiment (WOCE) data, J. Geophys. Res., 108, C1, 3007, doi:10.1029/2001JC001115, 2003.
Stammer, D., Ueyoshi, K., Köhl, A., Large, W. G., Josey, S. A., and Wunsch, C.: Estimating air-sea fluxes of heat, freshwater, and momentum through global ocean data assimilation, J. Geophys. Res., 109, C5, C05023, doi:10.1029/2003JC002082, 2004.
Tandon, A. and Zhao, L.: Mixed layer transformation for the North Atlantic for 1990–2000, J. Geophys. Res., 109, C05018, doi:10.1029/2003JC002059, 2004.
Thierry, V., Mercier, H., Grit, C., Gaillard, F., and Autret, E.: Seasonal and interannual variability of the Subpolar Mode Waters in the North Atlantic. Abstract of poster presented at CLIVAR Workshop on “North Atlantic Thermohaline Circulation variability”. Kiel, Germany,

13–16 September 2004 (see http://www.ifm.uni-kiel.de/allgemein/naw2004.htm), 2004.
Tsimplis, M. S. and Bryden, H. L.: Estimation of the transports through the Strait of Gibraltar, Deep-Sea Research I, 47, 2219–2242, 2000.
Tziperman, E.: On the role of interior mixing and air-sea fluxes in determining the stratification and circulation of the oceans, J. Phys. Oceanogr., 16, 680–693, 1986.
Valdivieso da Costa, M., Mercier, H., and Tréguier, A. M.: Effects of the mixed layer time variability on kinematic subduction rate diagnostics, J. Phys. Oceanogr., in press, 2005.
Walin, G.: On the relation between sea-surface heat flow and thermal circulation in the ocean, Tellus, 34, 187–195, 1982.
Wood, R. A., Keen, A. B., Mitchell, J. F. B., and Gregory, J. M.: Changing spatial structure of the thermohaline circulation in response to atmospheric CO2 forcing in a climate model, Nature, 399, 572–575, 1999.
Wu. P., Wood, R. A., and Stott, P.: Does the recent freshening trend in the North Atlantic indicate a weakening thermohaline circulation?, Geophys. Res. Lett., 31, L02301, doi:10.1029/2003GL018584, 2004.

Table 1. Total transports (Sv) across OCCAM sections. Positive values indicate northward transports across the zonal and quasi-zonal sections, and eastward transports across GibSt. "Light" and "Dense" refer to total northward/eastward and southward/westward transports, respectively.

Section	Light	Dense	Net
A5	26.01	−26.85	−0.83
A3	24.10	−25.18	−1.08
GibSt	1.17	−1.12	0.05
A25	20.10	−19.61	0.49
AR7W	13.52	−14.97	−1.45
EEL-64N	15.29	−14.90	0.39

OSD
2, 63–104, 2005

Table 2. Total transports (Sv) across observed sections.

Section	Light	Dense	Net
A5	31.03	−31.03	0.00
A25	23.74	−24.14	−0.40

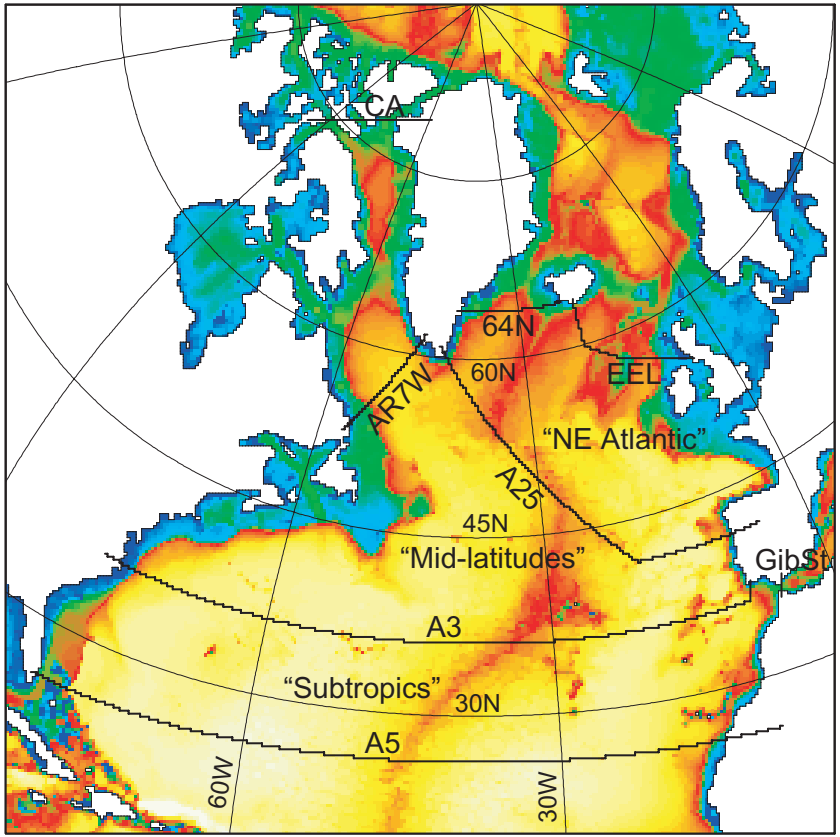

Fig. 1. The extra-tropical North Atlantic of OCCAM, showing model bathymetry and the major model sections (indicated in bold), which follow the sides of gridcells to exactly capture model transports. The three enclosed regions are labelled. OCCAM uses a rotated grid to represent the North Atlantic and the Arctic. For orientation, meridians are shown at 30° intervals, and lines of latitude at 15° intervals.

OSD
2, 63–104, 2005

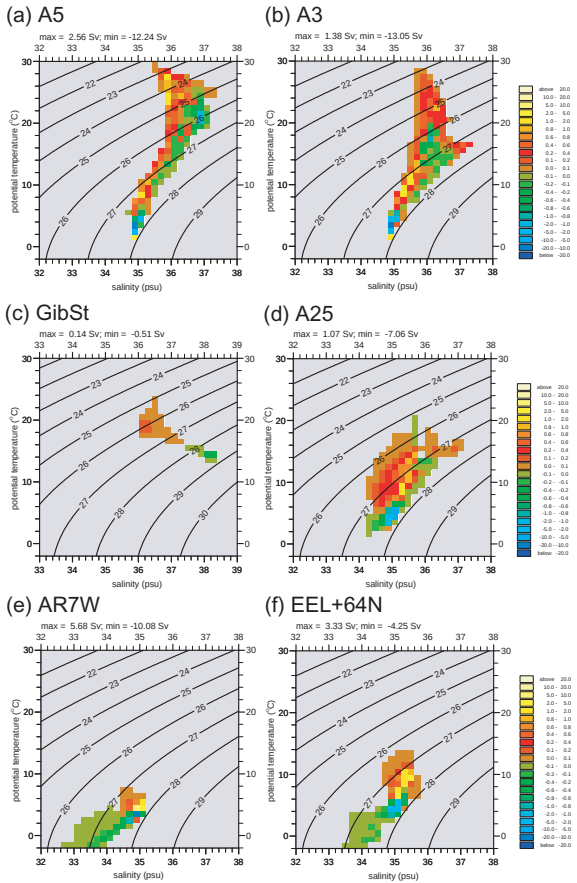

Fig. 2. Period-mean transports (units Sv, positive for northward flow) across each section partitioned in temperature and salinity: **(a)** A5; **(b)** A3; **(c)** GibSt; **(d)** A25; **(e)** AR7W; **(f)** EEL-64N. The contours indicate $\sigma_0(\theta, S)$. The salinity range in (c) is shifted +1 psu, in order to accommodate the high salinity MW. Transports in the range −0.01 to 0.01 Sv are grey-shaded.

OSD
2, 63–104, 2005

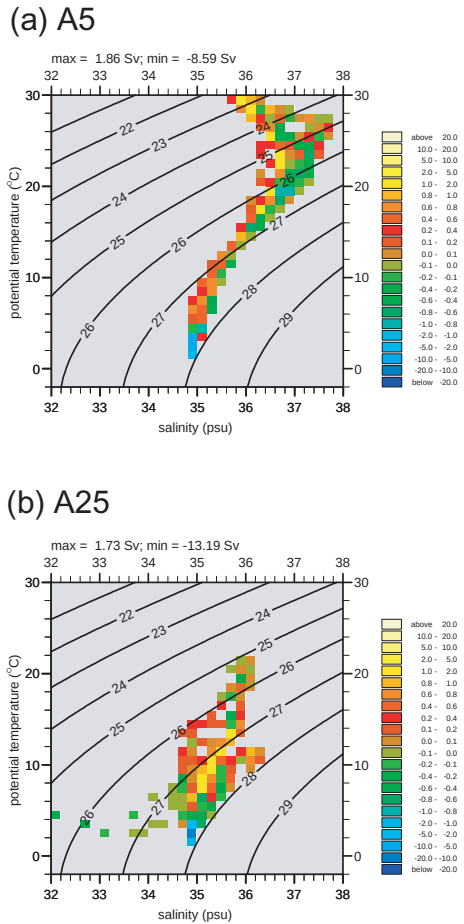

Fig. 3. As Fig. 2, based on estimates at: **(a)** A5 (June 1992); **(b)** A25 (August 1997).

OSD
2, 63–104, 2005

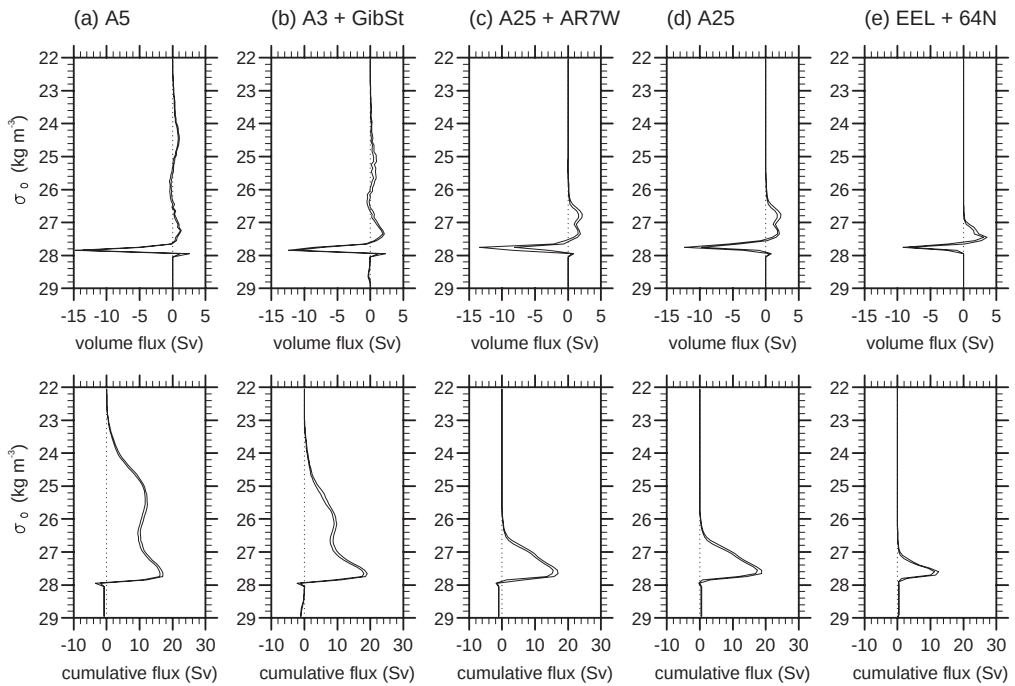

Fig. 4. Model transports partitioned according to potential density, σ_0, in "bins" of width 0.1 kg m^{-3}. Fluxes through the Gibraltar Straits are included with fluxes across A3. The sections A25 and AR7W are likewise considered together, as well as A25 separately. The two curves shown in each plot indicate a range of values due to interannual variability over 1985-2002, according to positive and negative excursions from the period-mean by two standard deviations. The upper panels show fluxes, the lower panels show cumulative transport, obtained by summing the fluxes, from low to high values of σ_0.

OSD
2, 63–104, 2005

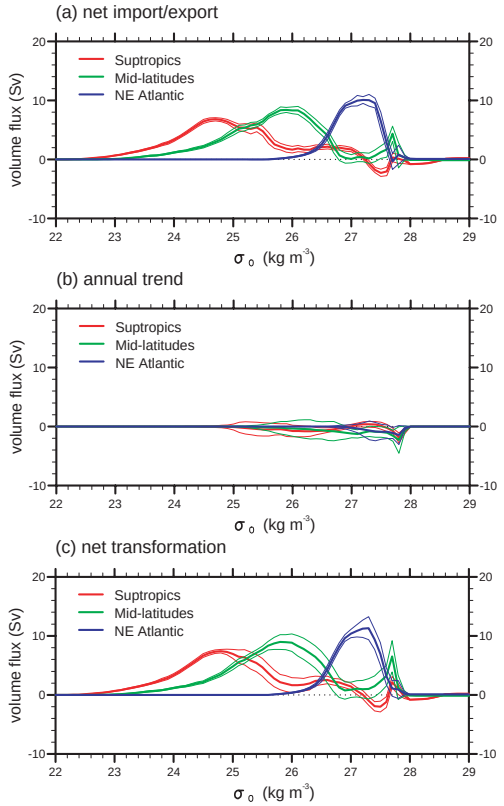

Fig. 5. Period-mean volume fluxes as a function of σ_0, in the three bounded regions, the Subtropics (red curve), Mid-latitudes (green curve), and NE Atlantic (blue curve): **(a)** due to import/export; **(b)** due to annual trend; **(c)** net transformation. Mean fluxes are indicated by solid lines. Thin lines indicate positive and negative excursions of two standard deviations. Positive fluxes indicate net import in (a), net accumulation in (b), and net transformation towards higher density in (c).

OSD
2, 63–104, 2005

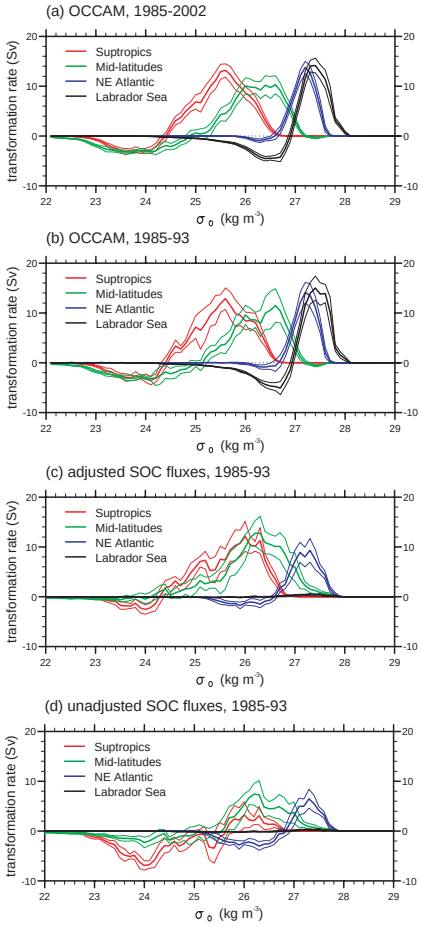

Fig. 6. As Fig. 5, showing surface water mass transformation rates in the three Atlantic Boxes and the Labrador Sea: **(a)** OCCAM, 1985–2002; **(b)** OCCAM, 1985–1993; **(c)** adjusted SOC, 1985–1993; **(d)** unadjusted SOC, 1985–1993.

OSD
2, 63–104, 2005

Water mass transformation in the North Atlantic

R. Marsh et al.

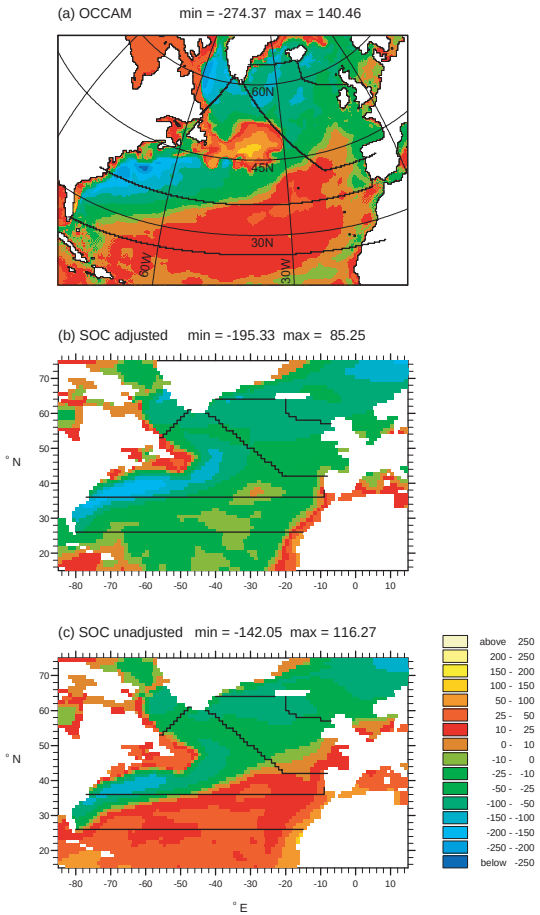

Fig. 7. Net surface heat flux (Wm^{-2}) in the North Atlantic, averaged over 1985–1997: **(a)** OCCAM; **(b)** SOC adjusted fluxes; **(c)** SOC unadjusted fluxes. The sections bounding each region are indicated. The OCCAM fluxes are shown on the same rotated grid as in Fig. 1.

OSD
2, 63–104, 2005

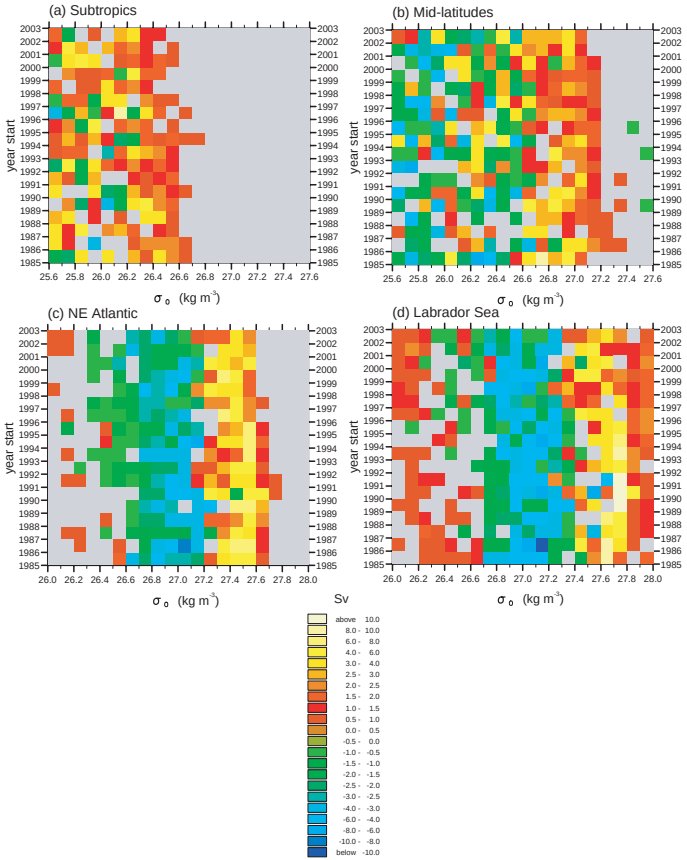

Fig. 8. Hovmuller plots of surface water mass formation rate in each σ_0-interval over limited ranges corresponding to formation of selected water masses: **(a)** STMW1 in the Subtropics Box; **(b)** STMW2 in the Mid-latitudes Box; **(c)** SPMW in the NE Atlantic Box; **(d)** LSW in the Labrador Sea. Formation rates in the range −0.5 to 0.5 Sv are grey-shaded.

OSD
2, 63–104, 2005

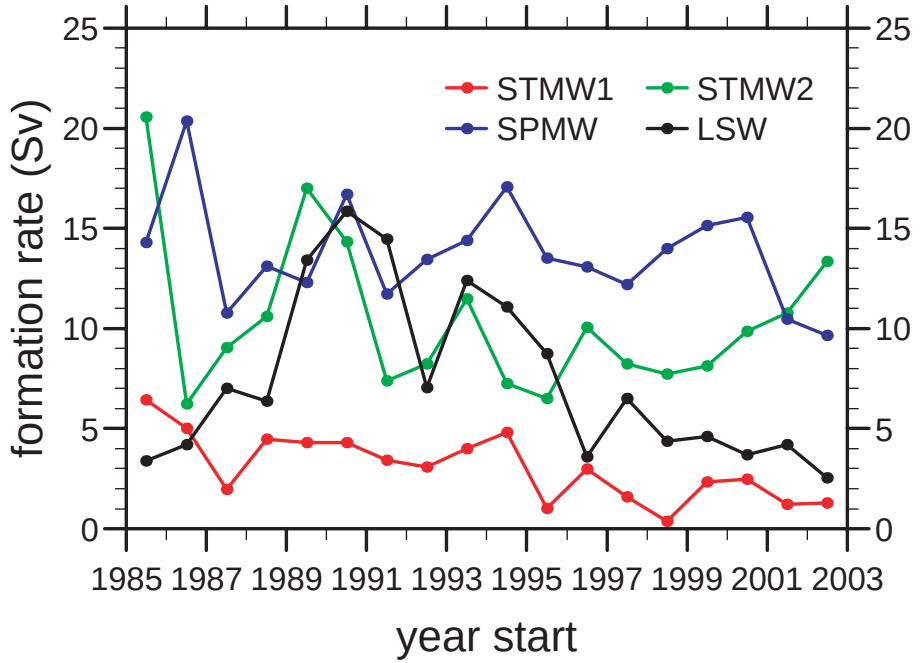

Fig. 9. Time series of the formation rates of STMW1 in the Subtropics Box (red curve), STMW2 in the Mid-latitudes Box (green curve), SPMW in the NE Atlantic Box (blue curve) and LSW in the Labrador Sea (black curve).

OSD
2, 63–104, 2005

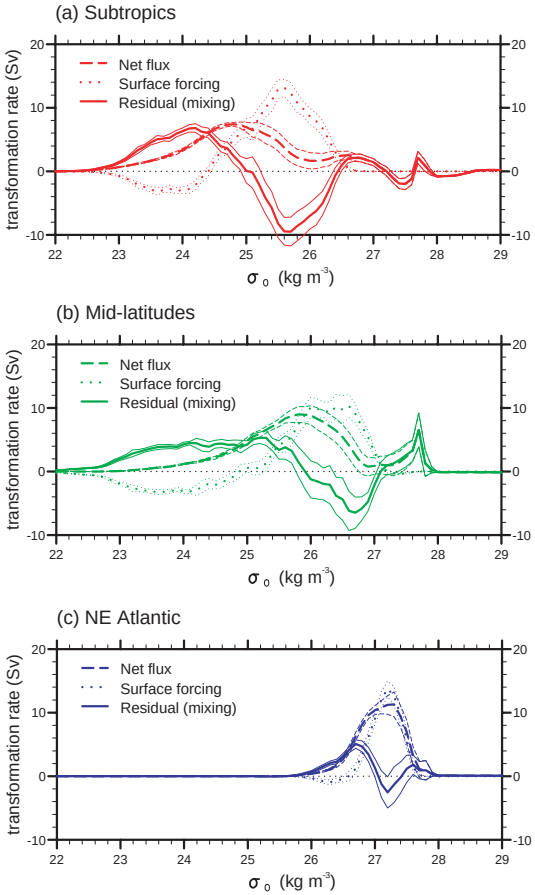

Fig. 10. As Fig. 5, showing transformation rates due to mixing (solid curves), obtained as a residual term between net transformation rates (dashed curves) and surface forced transformation rates (dotted curves): **(a)** Subtropics; **(b)** Mid-latitudes; **(c)** NE Atlantic.

OSD
2, 63–104, 2005

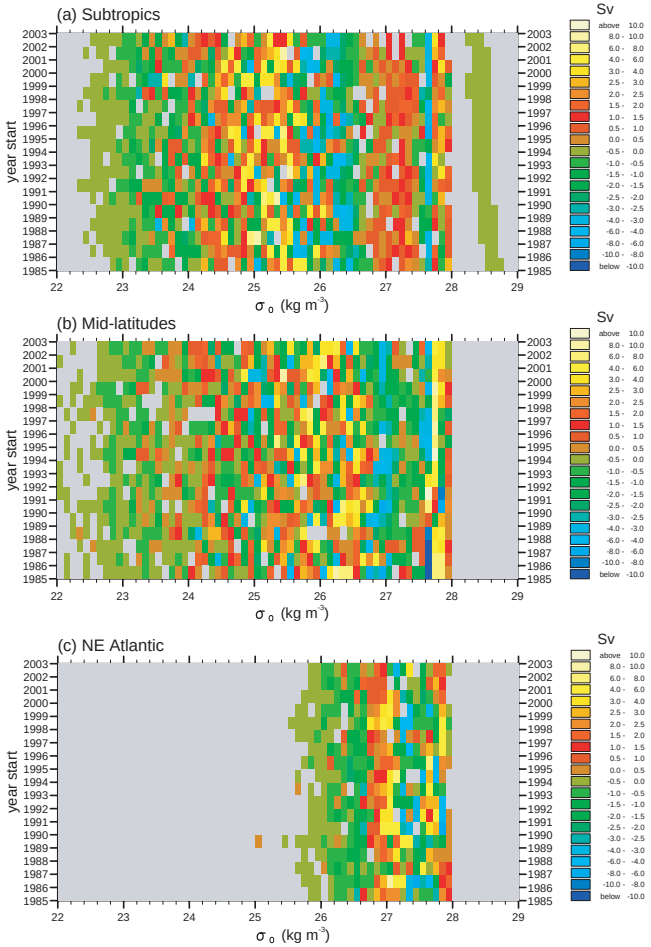

Fig. 11. Hovmuller plots of water mass formation rates due to mixing (as Fig. 7): **(a)** Subtropics; **(b)** Mid-latitudes; **(c)** NE Atlantic. Formation rates in the range −0.1 to 0.1 Sv are grey-shaded.

OSD
2, 63–104, 2005

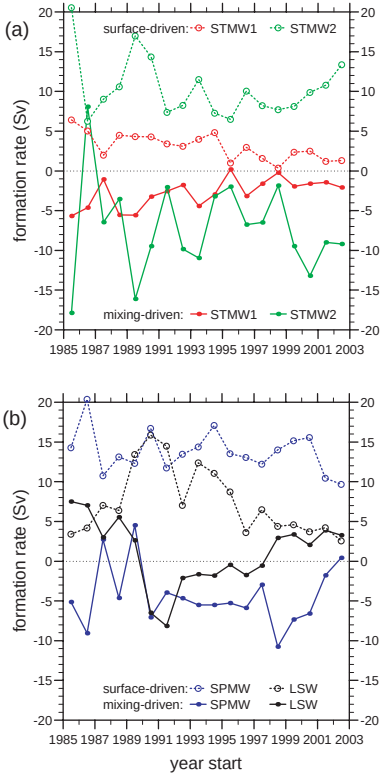

Fig. 12. Time series of formation rates due to mixing of: **(a)** STMW1 in the Subtropics Box (red solid curve), STMW2 in the Mid-latitudes Box (green solid curve); **(b)** SPMW in the NE Atalntic Box (blue solid curve) and dense LSW ($27.8<\sigma_0<27.9\,\mathrm{kg\,m^{-3}}$) in the Mid-latitudes Box (black solid curve). Negative formation rates correspond to consumption. The formation rates for each water mass (as Fig. 9) are indicated by dotted curves.

OSD
2, 63–104, 2005